

# Selective Adsorption of Ions with Different Diameter and Valence at Highly Charged Interfaces<sup>†</sup>

Mónika Valiskó

Department of Physical Chemistry, University of Pannonia, H-8201 Veszprém, P.O. Box 158, Hungary

Dezso Boda\*

Department of Molecular Biophysics and Physiology, Rush University Medical Center, Chicago, Illinois 60612, and Department of Physical Chemistry, University of Pannonia, H-8201 Veszprém, P.O. Box 158, Hungary

Dirk Gillespie

Department of Molecular Biophysics and Physiology, Rush University Medical Center, Chicago, Illinois 60612

Received: May 14, 2007; In Final Form: August 8, 2007

Monte Carlo simulation and density functional theoretical (DFT) results are reported for the selective adsorption of two competing cationic species at a highly charged planar interface. The two cations differ in both their diameter (2 and 4.25 Å) and valence (mono- and divalent). Our results show that in general the smaller or the divalent cation is preferentially adsorbed at the electrode. In the case when the divalent ion is larger and the monovalent ion is smaller, we find a competitive situation: at lower surface charges the electrostatic advantage of the divalent ions dominates, whereas at higher surface charges the entropic advantage of the small ions dominates. We show results for the excess adsorption, density profiles, and mean electrical potential in various situations where charge inversion occurs when divalent ions are present. Using the DFT decomposition of the chemical potential into various terms (e.g., ideal, electrostatic, hard sphere), we demonstrate that the competition between ionic species of different sizes and valences originates in the balance of excluded volume and electrostatic terms.

## 1. Introduction

The selective adsorption of ions of different diameters and valences at highly charged interfaces is studied using Monte Carlo (MC) simulations and density functional theory (DFT). Ion selectivity has a fundamental technological importance involving ion selective electrodes, ion exchange equipments, filters, and sensors.<sup>1</sup> Membranes that selectively allow the permeation of specific ions have an important role in these techniques. One of the most obvious examples of such a membrane is the biological plasma membrane of cells. Because the lipid bilayer is impermeable to ions, the selective transport of ions through the membrane is facilitated by membrane proteins that have a huge diversity in their structure, working mechanism, and physiological role. Ion channels, for example, allow the passive transport of specific ions down their electrochemical gradients whenever they get a proper signal to open.<sup>2</sup> Other important biological examples are calcium binding proteins like calsequestrin that selectively bind ions from a solution where that specific ion might be present only at nanomolar concentrations.

The mechanism by which all of these systems discriminate between ions might be very different. Adsorption on a surface, for example, can be physical in nature when the molecules are bound by weak van der Waals forces, whereas chemical adsorption occurs when stronger bonds (hydrogen or covalent)

are formed between the adsorbed molecules and the surface. In this work, we consider another kind of force that adsorbs ions near a charged surface: the electrostatic force. Specifically, we are interested in the case when the interface is highly charged so that the ions accumulate in the double layer (DL) at a high ionic density. In such a case, the size of the ions is very important and a competition between the two counter-ion species that might have different charges and different sizes occurs.

The electrical DL appears whenever an ionic solution is in contact with a surface of an electrode, a membrane, or a macromolecule, and so forth. The diffuse layer formed by counter-ions and co-ions extends into the electrolyte and plays a crucial role in the dynamics of electrochemical reactions and ion transport. Considerable effort has been employed to explain the structure of this region. The first attempt to describe the diffuse layer was that of Gouy,<sup>3</sup> Chapman,<sup>4</sup> and Stern<sup>5</sup> using the Poisson–Boltzmann (PB) treatment of point ions embedded in a continuum solvent. Because of its simplicity, this theory is widely used in many fields such as biophysics, solution chemistry (where it is known as Debye–Hückel theory<sup>6</sup>), and colloid chemistry (where it is known as Derjaguin–Landau–Verwey–Overbeek theory<sup>7,8</sup>). The limitations of the PB theory are well-known;<sup>9</sup> most importantly, because the ions have finite size, it is applicable only in dilute solutions.

The analytical form of the PB theory, nevertheless, still makes it a popular method for describing experimental phenomena, for example when the treatment of the DL structure is coupled to equations of electrochemical hydrodynamics.<sup>10–12</sup> Steric effects were taken into account in many works<sup>13–16</sup> by adding

<sup>†</sup> Part of the “Keith E. Gubbins Festschrift”.

\* Author to whom correspondence should be addressed. E-mail address: dezso\_boda@rush.edu.

excess excluded volume terms to the chemical potential (see also the references in the paper of Kilic et al.<sup>10</sup>) while still treating electrostatics on the mean field level. Electrostatic correlations beyond the mean field approximation have been added in more-advanced modifications of the PB theory.<sup>17–20</sup> The finite size of ions is naturally included in modern statistical mechanical theories such as the mean spherical approximation,<sup>21,22</sup> integral equations,<sup>23–25</sup> and DFT.<sup>26</sup> Lately, computer simulation has become a standard tool that is able to treat models of the DL that are not accessible to theories (see the review of Spohr<sup>27</sup> and references therein).

The case when different counter-ions are present in the DL has captured the attention of many groups in the past few years because of the importance of *overcharging* in many applications. *Overcharging* in the DL around charged macroparticles (such as proteins, DNA, colloidal suspensions, etc.) means that more counter-ions are attracted to the immediate vicinity of the surface of the particle than necessary to compensate the charge of the particle.<sup>28,29</sup> Consequently, a layer with excess co-ions appears, a phenomenon also called *charge inversion*. This phenomenon is fundamental in explaining the attractive forces acting between like-charged particles.<sup>30,31</sup> Adding multivalent ions to the solution changes the structure of the DL, which, in turn, changes the long range behavior of the solution. For example, adding spermine (+3 valence) or spermidine (+4 valence) to DNA solution causes DNA condensation (salting out); adding even more of these cations, the DNA is redissolved.<sup>32–35</sup> The phenomenon was reproduced by simulations for rodlike<sup>30,31</sup> and spherical<sup>36</sup> macro-ions using the primitive model of electrolytes. These studies showed that the stability of macro-ion solutions and the aggregation mechanism can be explained solely by electrostatic correlation forces without any need to involve specific van der Waals attractions. PB theory is unable to account for *overcharging* because it is closely related to the presence of multivalent ions and excluded volume effects.

A great deal of work has been done in various communities on ions of different valences and sizes at charged interfaces using the continuum dielectric solvent approach. To place this work into context, we briefly review this body of work:

Martín-Molina et al.<sup>37–40</sup> studied the role of the structure of the DL and *charge inversion* in the reversal of the sign of the electrophoretic mobility. Their simulations for the DL containing monovalent and trivalent counter-ions showed the importance of ion size correlations, and a qualitative agreement with electrophoretic measurements was found.

Delville et al.<sup>41</sup> studied the competitive condensation of monovalent and trivalent counter-ions between the charged lamellae of clay materials. Their simulations led to conclusions that are in agreement with those of this study. They showed that the clay surfaces preferred counter-ions of larger charge, a selectivity that was enhanced by an increase in the charge of the interfaces. Their results quantified the possibility of using clay materials as ion exchangers.

Jönsson et al.<sup>42,43</sup> showed that the primitive model can explain the interaction between calcium-silicate-hydrate particles that constitute cement paste. These particles have unusually high surface charges (0.4–0.8 Cm<sup>-2</sup>) because of the high OH<sup>-</sup> concentration (pH 10–13). These charges are compensated by Ca<sup>2+</sup> ions. The presence of high surface charge and Ca<sup>2+</sup> is sufficient to explain the cement cohesion. They showed that the cohesion becomes weaker with the addition of enough Na<sup>+</sup> salt. Labbez et al.<sup>44</sup> obtained good agreement between experimental and simulated results for the surface charge and

electrokinetic behavior of calcium-silicate-hydrate and confirmed that “the dielectric continuum model has a sound physical basis.”

Wang et al.<sup>45,46</sup> investigated the competitive binding of counter-ions of the same valence but different diameter to DNA molecules. They found that smaller cations have stronger competitive ability in accordance with the results of this work.

Woelki and Kohler<sup>18</sup> developed a modified Poisson–Boltzmann equation, which includes the effects of the finite size of ions, dielectric saturation, ionic polarization, and the self-atmosphere energy of the ions. They obtained that Br<sup>-</sup> ions are preferred over the larger and divalent SO<sub>4</sub><sup>2-</sup> ions at high enough surface charges even if the concentration of the former is much smaller.<sup>19</sup> Because many of the effects considered by this theory are not included in our simple model of the DL, a direct comparison cannot be made between the results of Woelki and Kohler and the present work. In the qualitative trends, however, we agree.

Taboada-Serrano et al.<sup>47</sup> also considered mixtures of counter-ions of different valences and sizes. They used discrete charges on the interface instead of a continuous surface charge. Their findings are in good agreement with our results. They also found<sup>48</sup> that the compositions, sizes, and valences of counter-ions in the overlapping DL between like-charged macroparticles play a determining role in the force acting between the two macroparticles.

The studies discussed above clearly show the usefulness of the primitive model of electrolytes in these situations. This is probably the consequence of the fact that these phenomena are rather determined by the structure of the diffuse layer in relatively diluted electrolyte solutions. The continuum model of the solvent seems appropriate in these cases.

Our previous studies on the electrical DL containing ions of different valences and sizes were mainly interested in the case when the electrode charge is zero or small.<sup>49,50</sup> The potential at the point of zero charge is a result of the balanced competition of the charge and size asymmetry of the cations and the anions. We have studied this with MC simulations,<sup>49</sup> and in a second paper<sup>50</sup> it was shown that the DFT of Gillespie et al.<sup>51,52</sup> was able to capture the essential properties of this system very accurately.

In this work, we give a systematic study of the DL where the two competing cations at a negatively charged surface have different diameters (2 or 4.25 Å) and valences (1 or 2). We study the effect of the surface charge and the composition of the electrolyte. We analyze our results in terms of ionic profiles, excess adsorption, and electrical potential. Additionally, we use the advantageous feature of the DFT to naturally separate the various terms of the chemical potential corresponding to ideal gas, mean-field part of electrostatics, electrostatic correlations, and hard-sphere exclusion. We show how the competition of these terms is responsible for the selectivity of the interface for the competing counter-ions. With this method, we quantify the mechanism of ion selectivity and show that it is governed by the competition of hard-sphere exclusion and electrostatic terms.

This mechanism was proposed to explain the high Ca<sup>2+</sup> versus Na<sup>+</sup> selectivity of calcium channels by Nonner et al.<sup>53,54</sup> The small selectivity filter of calcium-selective ion channels has four negatively charged carboxyl groups that makes the filter highly charged and crowded. These negative charges attract cations in the filter that will prefer Ca<sup>2+</sup> because it provides twice the charge as Na<sup>+</sup> does while occupying about the same volume. Furthermore, it was shown that these types of filters prefer smaller ions if the valences of the competing ions are the

same.<sup>53,55</sup> The key feature of the mechanism is the high ionic density in the filter, which is similar to the planar case considered in this work where the region near the interface is also crowded. Although the geometry is different, the driving force behind selectivity, the competition of entropic repulsion and electrostatic attraction, nevertheless, is the same.

## 2. Model and Methods

**2.1. Model.** We consider the primitive model of an electrolyte near a hard, planar, charged surface. The solvent is implicitly described by a dielectric constant  $\epsilon = 78.4$  that is uniform throughout the system. The ions are modeled as charged, hard spheres so that the interaction potential between ions of species  $i$  and  $j$  is

$$u_{ij}(r) = \begin{cases} \infty & \text{for } r \leq d_{ij} \\ \frac{z_i z_j e^2}{4\pi\epsilon\epsilon_0 r} & \text{for } r > d_{ij} \end{cases} \quad (1)$$

where  $e$  is the fundamental charge,  $\epsilon_0$  is the permittivity of vacuum,  $r$  is the distance between the two ions,  $z_i$  and  $d_i$  are the valence and diameter, respectively, of ion species  $i$ , and  $d_{ij} = (d_i + d_j)/2$ . The ion–wall interaction potential is

$$u_i(x) = \begin{cases} \infty & \text{for } x \leq d_i/2 \\ -\frac{z_i e\sigma}{2\epsilon\epsilon_0 x} & \text{for } x > d_i/2 \end{cases} \quad (2)$$

where  $\sigma$  is the surface charge density of the wall and  $x$  is the distance of the ion from the wall. In our calculations, the temperature was  $T = 298.15$  K.

**2.2. Density Functional Theory.** The DFT we use is described in detail in earlier papers.<sup>51,52</sup> Here, we briefly summarize it.

The excess free energy is decomposed into two terms: the hard-sphere (HS) and electrostatic (ES) excess free energy functionals. For the HS functional  $F_{HS}$ , we use the “antisymmetrized” excess free energy density.<sup>56</sup>

Perturbation methods approximate  $F_{ES}[\{\rho_k(y)\}]$  with a functional Taylor series, truncated after the quadratic term, expanded around a reference fluid:

$$\begin{aligned} F_{ES}[\{\rho_k(y)\}] &\approx F_{ES}[\{\rho_k^{\text{ref}}(y)\}] - \\ &kT \sum_i \int c_i^{(1),ES}[\{\rho_k^{\text{ref}}(y)\};x] \Delta\rho_i(x) dx - \\ &\frac{kT}{2} \sum_{ij} \int \int c_{ij}^{(2),ES}[\{\rho_k^{\text{ref}}(y)\};x,x'] \Delta\rho_i(x) \Delta\rho_j(x') dx dx' \end{aligned} \quad (3)$$

with

$$\Delta\rho_i(x) = \rho_i(x) - \rho_i^{\text{ref}}(x) \quad (4)$$

where  $\rho_i^{\text{ref}}(x)$  is a given (and possibly inhomogeneous) reference density profile and  $c_i^{(1),ES}$  and  $c_{ij}^{(2),ES}$  are the first- and second-order direct correlation functions (DCF), respectively. Previous DFTs have made this reference density profile just the bulk reference density<sup>57,58</sup> and have been applied to various problems.<sup>59,60</sup> The RFD approach makes the reference fluid densities functionals of the particle densities  $\rho_i(x)$ :<sup>52</sup>

$$\bar{\rho}_k^{\text{ref}}(y) = \bar{\rho}_k[\{\rho_i(x)\};y] \quad (5)$$

$\bar{\rho}_k$  is the RFD functional, recalling its origin as a “reference fluid

density.” It was shown<sup>52</sup> that the first-order DCF is given by

$$c_i^{(1),ES}(x) = -\frac{1}{kT} \frac{\delta F_{ES}}{\delta \rho_i(x)} \quad (6)$$

$$\approx \bar{c}_i^{(1),ES}(x) + \sum_j \int \bar{c}_{ij}^{(2),ES}(x,x') \Delta\rho_j(x') dx' \quad (7)$$

where

$$\Delta\rho_k(x) = \rho_k(x) - \bar{\rho}_k(x) \quad (8)$$

$$\bar{c}_i^{(1),ES}(x) = c_i^{(1),ES}[\{\bar{\rho}_k(y)\};x] \quad (9)$$

and

$$\bar{c}_{ij}^{(2),ES}(x,x') = c_{ij}^{(2),ES}[\{\bar{\rho}_k(y)\};x,x'] \quad (10)$$

For the RFD functional, the densities  $\bar{\rho}_k(x)$  must be chosen so that both the first- and second-order DCFs can be estimated. This is possible because the densities  $\{\bar{\rho}_k(x)\}$  are a mathematical construct and do not represent a physically real fluid. The particular choice of the RFD functional we use here is<sup>51,52</sup>

$$\bar{\rho}_i[\{\rho_k(x')\};x] = \frac{3}{4\pi R_{ES}^3(x)} \int_{|x'-x| \leq R_{ES}(x)} \alpha_i(x') \rho_i(x') dx' \quad (11)$$

where the  $\{\alpha_k\}$  are chosen so that the fluid with density  $\{\alpha_k(x)\}$   $\rho_k(x)$  is charge-neutral and has the same ionic strength as the fluid with density  $\{\rho_k(x)\}$  at every point  $x$ . The radius of the sphere  $R_{ES}(x)$  over which we average is the local electrostatic length scale. Specific formulas for  $\alpha_k(x)$  and  $R_{ES}(x)$  are given elsewhere.<sup>51,52</sup> To estimate the electrostatic DCFs  $\bar{c}_i^{(1),ES}(x)$  and  $\bar{c}_{ij}^{(2),ES}(x,x')$  at each point, we use a bulk formulation (specifically the MSA) at each point  $x$  with densities  $\bar{\rho}_k(x)$ .<sup>61–63</sup>

As we will see, DFT is very successful in reproducing the MC results. The agreement is usually very good quantitatively (but always, at least, qualitatively) and better for the smaller and monovalent ions. This RFD functional has also been used by Sokołowski et al. to create a (nonperturbative) weighted density approximation electrostatic functional.<sup>64,65</sup> They applied the energy route of the MSA to define  $F_{ES}$  as a functional only of the  $\{\bar{\rho}_k(x)\}$ . Their approach successfully described the phase behavior of the restricted primitive model (RPM) of electrolytes in pores<sup>64</sup> and the anomalous temperature dependence of the capacitance of the electrical DL of the RPM.<sup>65</sup>

**2.3. Monte Carlo Simulations.** For the MC simulations, we use the canonical (constant  $NVT$ ) ensemble in a simulation cell with periodic boundary conditions in the directions parallel to the interface. In the perpendicular direction, the cell is confined by a uniformly charged hard wall on the left side and by a neutral hard wall on the right side, spaced far enough apart for a homogeneous fluid to exist in the middle of the cell. This length of the cell varied between 50 and 105 Å, depending on the desired bulk ion concentration. In the other dimensions, the width of the cell varied between 40 and 60 Å. The number of particles was 300–500, depending on cell size and desired bath concentration. The lengths of the simulations varied between 150 000 and 600 000 MC cycles; in one cycle  $N_{\text{tot}}$  particle displacement was attempted, where  $N_{\text{tot}}$  is the total number of ions in the simulation cell. The effect of ions in the periodic replicas of the central simulation cell was taken into account by the charged sheet method.<sup>66</sup> The applicability of this method

has been thoroughly tested in the case of aqueous electrolytes by extensive system-size checks. Details of the MC simulation methods are given elsewhere.<sup>49</sup>

### 3. Results and Discussion

**3.1. Excess Adsorption as a Function of the Surface Charge and Composition of Counter-ions.** There are several choices to characterize the ability of various ions to be adsorbed to the wall. One possibility is to use the contact value of various ions at the surface. This is a local, though quite important quantity underlying contact theorems.<sup>67</sup> The excess adsorption, which is an integral quantity, is more accessible to measurements. The electrical potential is another quantity that can be related to experiments through electrophoretic measurements.

We choose the excess adsorption of charge (or, just adsorption from now), the integral of the difference of the concentration profile  $\rho_i(x)$ , and the bulk concentration  $\rho_i^b$  multiplied by the fundamental charge:

$$\Gamma_i = e \int_{x=0}^{\infty} [\rho_i(x) - \rho_i^b] dx \quad (12)$$

The unit of this adsorption is  $\text{Cm}^{-2}$ . The sum of these adsorption values for the various ionic species weighted by their valences gives the negative of surface charge of the electrode:

$$\sum_i z_i \Gamma_i = -\sigma \quad (13)$$

Thus, plots of  $\Gamma_i$  against  $\sigma$  show the shares of the various species from balancing the electrode charge indicated on the abscissa.

In all calculations, the diameter of the anion was  $d_- = 2 \text{ \AA}$ , and the diameter of the small and large cations were 2 and 4.25  $\text{ \AA}$ , respectively. The choice of the diameter of the anion does not have an important effect (data not shown). Monovalent and divalent cations were considered, and the valence of anions was always  $-1$ . In one part of our calculations, the composition of the electrolyte was fixed (equimolar for the cations) and the surface charge was varied between  $-1.5$  and  $0.5 \text{ Cm}^{-2}$ . In the other part of our calculations the surface charge was fixed and the composition of cations was varied with the concentration of the anions unchanged. Such high charge densities can occur locally at protein binding sites, selectivity filters of channels, or places where deprotonation of certain groups is probable at appropriate pH. For example, charge density as high as  $-0.48 \text{ Cm}^{-2}$  appears in hydrated calciosilicates.<sup>68</sup> Using inert metals and a careful design of the electrochemical cell, an electrochemical reaction between the electrode and electrolyte solution can be prevented, the stability of the DL can be maintained, and relatively large electrode charges can be achieved.

Although the surface charge and thus the potential are limited in equilibrium systems, high values of the applied potential can occur in nonequilibrium or quasi-equilibrium situations. For example,  $\approx 100kT/e$  induced DL voltage can build and DLs crowded with counter-ions can form at microelectrodes in AC electro-osmotic experiments.<sup>10–12</sup> Nonlinear electrokinetic phenomena such as induced-charge electro-osmosis<sup>69</sup> play a fundamental role in microfluidic devices, microbatteries, and electrochemical sensors. The importance of steric effects in the crowded DLs at large applied voltages have been pointed out.<sup>10–12</sup> Simulation and theoretical methods able to account for electrostatic correlations (such as those used in this paper) might give an important contribution to understanding the dynamical response of the electrolyte to the large and quickly alternating electric fields present in these devices. Preliminary

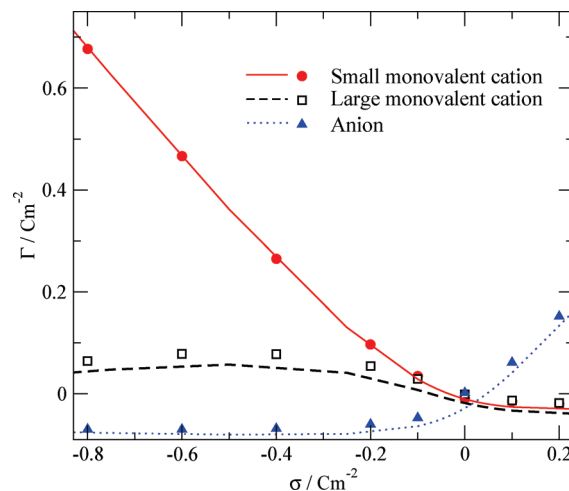


**Figure 1.** Excess adsorption of small monovalent cations (1 M concentration), large monovalent cations (1 M concentration), and anions (2 M concentration) as a function of the electrode charge. The lines and symbols represent DFT and MC results, respectively.

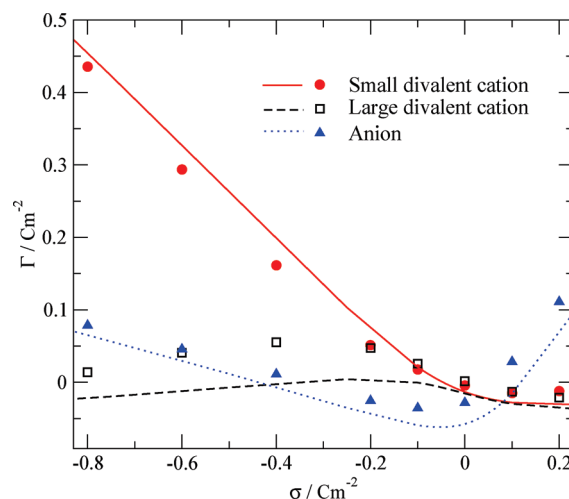


**Figure 2.** Excess adsorption of small divalent cations (1 M concentration), large divalent cations (1 M concentration), and anions (4 M concentration) as a function of the electrode charge. The lines and symbols represent DFT and MC results, respectively.

calculations in this voltage regime show reasonable agreement between MC and DFT results. Although DFT overestimates packing effects at the electrode, it gives a DL voltage similar to the MC result.

First, let us consider size selectivity when the only factor that can influence adsorption is the size of the ions. In Figure 1, the adsorption is shown as a function of the surface charge when a 1 M small and 1 M large monovalent cation is present in the bulk. Symbols and curves usually denote MC and DFT results, respectively, in this work. At positive surface charges, the anions are preferred because they are the counter-ions, whereas at negative surface charges the two cations compete for space near the interface. It is not a surprise that the smaller ions win this competition and are adsorbed at the electrode with greater efficiency. Their preference is more pronounced at higher surface charges.

In Figure 2, the same situation is shown for mixtures of 1 M small and 1 M large divalent ions. The principal feature that small ions are preferable is unchanged. The behavior of the large cations and the anions, nevertheless, is quite different from the monovalent case. As the surface charge becomes more negative, the number of anions increases and surpasses the number of

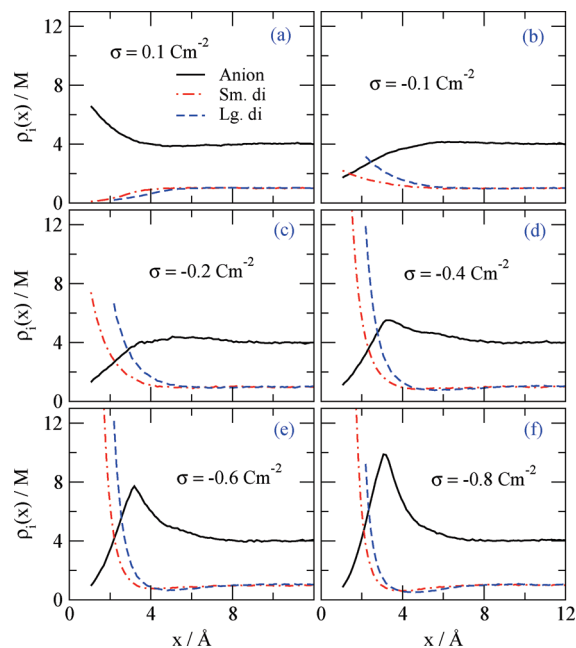


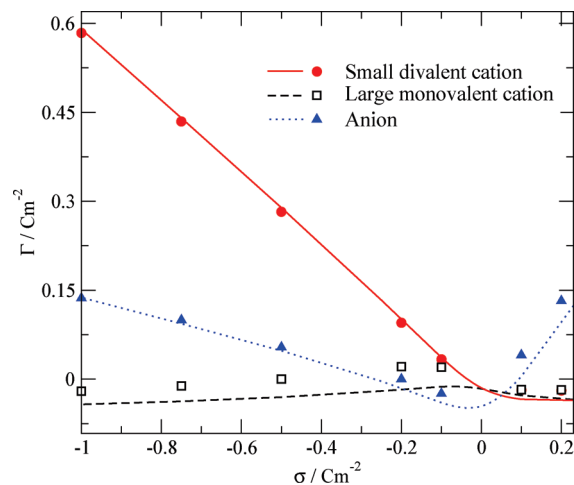
**Figure 3.** Concentration profiles of small divalent (Sm. di) cations (1 M concentration), large divalent (Lg. di) cations (1 M concentration), and anions (4 M concentration) for different electrode charges as obtained from MC simulations.

the large cations whose number decreases after going through a maximum. The explanation is that the association of a small divalent cation with anions have a higher probability. As the number of small divalent cations increases, they bring the associated anions with them. The large cations are excluded from the DL region as the density increases despite the fact that they are attracted by the negatively charged wall. As the surface charge increases, the first layer at the interface is occupied by the small cations and a peak of anions builds in the second layer that gradually becomes larger than the contact value of the large cations (Figure 3).

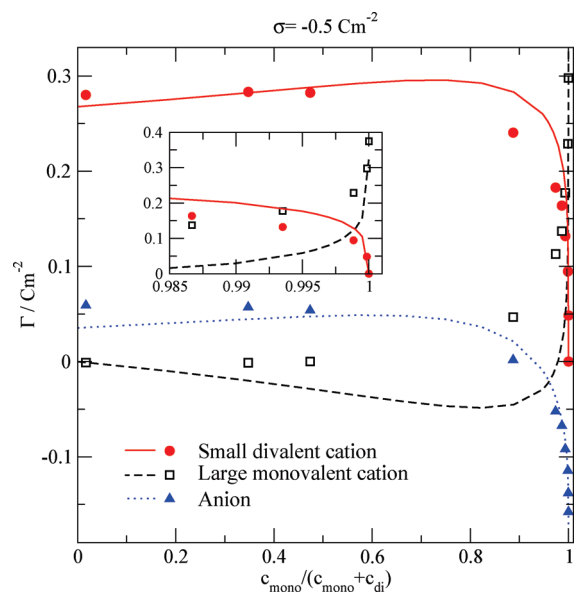
The next step would be the case where the size of the cations is the same while their valence is different. This case corresponds to the  $\text{Ca}^{2+}$  versus  $\text{Na}^+$  selectivity that was extensively studied before in different geometries.<sup>55,70–73</sup> The main result of these studies that the divalent ions have the advantage in highly charged, high-density regions remains valid in the planar geometry. Our results for the planar geometry (not shown) confirm the conclusions drawn from the cylindrical geometry. Moreover, the case of counter-ions with different charges but with the same size was considered in most of the papers cited in the Introduction.

Figure 4 shows the adsorption results for the case when 1 M small divalent and 1 M large monovalent cations are present in the system. Comparing this figure to Figure 2, it is apparent that the small divalent cations compete against the large monovalent cations *more* efficiently than against the large divalent cations. Alternatively, comparing this figure to Figure 1, it is apparent that the large monovalent cations compete against the small divalent cations *less* efficiently than against the small monovalent cations. The two effects, smaller size and larger charge, strengthen each other in the small divalent versus large monovalent case of Figure 4. At large surface charges, the adsorption of the large monovalent cations even becomes negative.

These results indicate a high small-divalent versus large-monovalent ion selectivity (we call this the *selective* case). To measure this selectivity, we performed a mole fraction experi-



**Figure 4.** Excess adsorption of small divalent cations (1 M concentration), large monovalent cations (1 M concentration), and anions (3 M concentration) as a function of the electrode charge (the *selective* case). The lines and symbols represent DFT and MC results, respectively.



**Figure 5.** Excess adsorption of small divalent cations, large monovalent cations, and anions (3 M concentration, fixed) as a function of the cation mole fraction for electrode charge  $\sigma = -0.5 \text{ Cm}^{-2}$  (the *selective* case). The lines and symbols represent DFT and MC results, respectively. The inset magnifies the region close to the pure monovalent case.

ment where the surface charge was fixed at value  $\sigma = -0.5 \text{ Cm}^{-2}$ , the concentration of the anions was also kept constant at 3 M, and the relative quantity of the two cations was changed. The adsorption of the various species is shown in Figure 5 as a function of the mole fraction of the monovalent cation  $c_{\text{mono}} / (c_{\text{mono}} + c_{\text{di}})$ . The adsorption of small divalent cations is large for almost all compositions, whereas the adsorption of the large monovalent cations is close to zero (negative in DFT). The large monovalent cations start to surpass the small divalent cations at the interface only when their quantity becomes about 98% of the total number of cations. In the region where the divalent ions are preferred, there is a positive adsorption of anions, whereas it quickly becomes negative as the monovalent ions take over at the interface. The DFT data properly reproduce this strong selectivity.

The opposite case, when the divalent cations are large and the monovalent cations are small, is more interesting because there is a competition between the size and valence selectivity

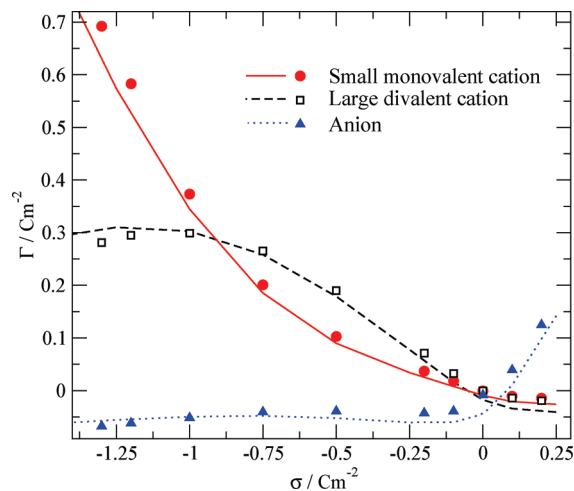


**Figure 6.** Excess adsorption of small monovalent cations (1 M concentration), large divalent cations (1 M concentration), and anions (3 M concentration) as a function of the electrode charge (the *competitive* case). The lines and symbols represent DFT and MC results, respectively.

(we call this the *competitive* case). Figure 6 shows the adsorption curves for a mixture of 1 M large divalent and 1 M small monovalent cations. Both cations are attracted to the interface while adsorption of the anions remains negative for negative surface charges. The divalent cations are attracted to the wall more strongly because the electrostatic attraction is twice as large as that for the monovalent ions, but the small monovalent cations are preferred at high electrode charge because they can find space more easily in the crowded region near the interface. For smaller surface charges, there is a first layer of small monovalent ions at the wall, but there are more large divalent cations in the second layer farther from the surface as seen from the concentration profiles in Figure 7a for  $\sigma = -0.5 \text{ Cm}^{-2}$  (note the logarithmic scale). The competition for space is not so strong in this case; therefore, the divalent ions have an electrostatic advantage despite their larger size. As the surface charge is increased (Figure 7b and c), the number of the small ions increases, whereas the number of the large ions shows saturation. This is because the smaller size of the monovalent ions allows them to produce a more dense packing. This higher density of closely packed ions produces a higher charge density than the large divalent cations despite the fact that they provide only one electronic charge with every ion situated at the electrode. The density profiles in Figure 7 show this first layer of small ions at the interface with a peak surpassing the peak of second layer of the large ions with increasing surface charge. Figure 7 shows both MC and DFT results; the agreement between them is very good. The right-hand side panels show the curves near the interface using a linear scale to illustrate the competition between the two cations better.

The mole fraction experiment similar to that in Figure 5 is shown in Figure 8 for two selected surface charges  $\sigma = -0.5$  and  $-1.25 \text{ Cm}^{-2}$ . The curves are much closer to linear, indicating a more balanced competition between the two cationic species than in the case of the small divalent versus large monovalent case (Figure 5). The position of the crosspoint is strongly influenced by the value of the surface charge. At a large negative surface charge, the small monovalent cations take over when their mole fraction is about 0.25 so the interface is selective for the small monovalent cation. In the case of  $\sigma = -0.5 \text{ Cm}^{-2}$ , the situation is reversed: the crosspoint occurs at a mole fraction larger than 0.5, so the interface is selective for the large divalent cation.

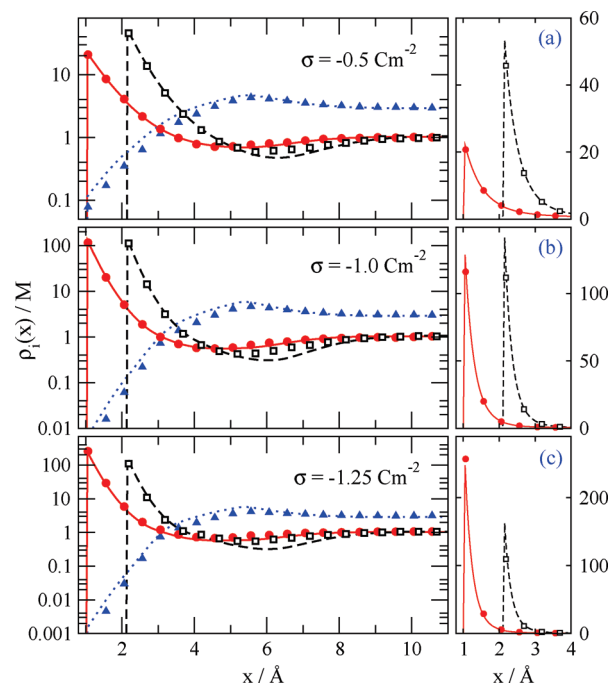


**Figure 7.** Concentration profiles of small monovalent cations (1 M concentration), large divalent cations (1 M concentration), and anions (3 M concentration) for different electrode charges as obtained from MC simulations and DFT (the *competitive* case). The meaning of symbols and curves is the same as those in Figure 6.

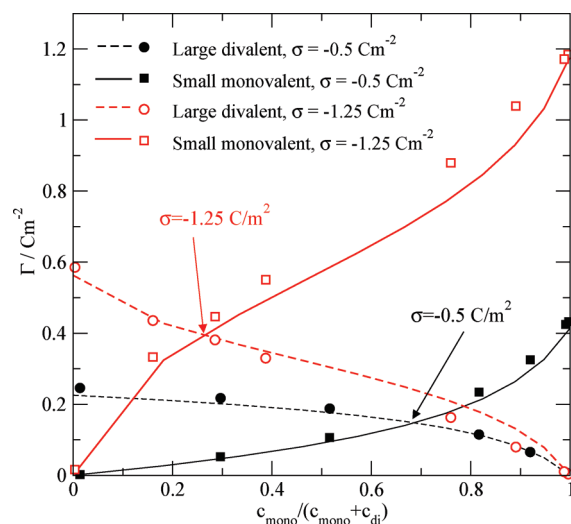


**Figure 8.** Excess adsorption of small monovalent cations, large divalent cations, and anions (3 M concentration, fixed) as a function of the cation mole fraction for electrode charges  $\sigma = -0.5$  and  $-1.25 \text{ Cm}^{-2}$  (the *competitive* case). The lines and symbols represent DFT and MC results, respectively.

This *competitive* case was also considered by Taboada-Serrano et al.<sup>47,48</sup> and by Woelki and Kohler.<sup>18,19</sup> Their investigations led to the same conclusions as ours: small ions adsorb better at the electrode than larger multivalent ions if the electrode charge is large. This phenomenon cannot be explained without the correct treatment of ion–ion correlations and hard-sphere exclusion effects.

**3.2. Electrostatic Potential.** The mean electrical potential profile is one of the most important features of DLs. Its sign reversal due to *charge inversion* farther from the first layer near the surface is one of the basic reasons for phenomena such as sign reversal of electrophoretic mobility and attractive interactions between like-charged macromolecules.<sup>28–40</sup> The potential

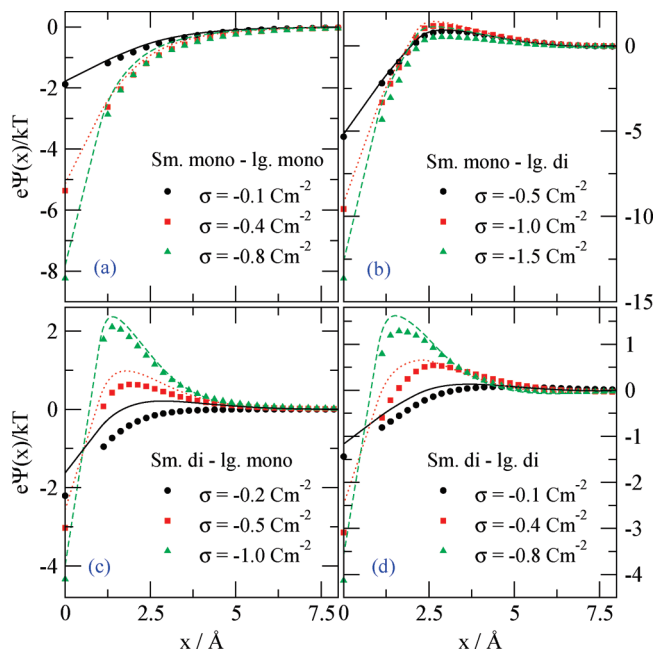


**Figure 9.** Mean electrical potential profiles for (a) small monovalent (Sm. mono) vs large monovalent (Lg. mono), (b) small monovalent vs large divalent, (c) small divalent vs large monovalent, and (d) small divalent vs large divalent cases for various surface charges. The concentration of each of the cations is 1 M in every case. The lines and symbols represent DFT and MC results, respectively.

profiles in the four cases studied in this work are shown for different surface charges in Figure 9. Although the profiles are monotonic for the small monovalent versus large monovalent case (Figure 9a), they show nonmonotonic behavior when divalent ions are present. These maxima are consequences of *overcharging* the electrode. We find the strongest effect in the *selective* case (Figure 9c): small divalent ions are more efficient in *overcharging* the electrode. The DFT results show good agreement with the MC data.

Electrophoretic mobility is generally related to the value of the potential at the contact position of the counter-ion. Because we have ions of different sizes, we plot the values of the potential at the electrode ( $x = 0$ , Figure 10a), at the contact position of the smaller ion ( $x = d_{sm}/2$ , Figure 10b), and at the contact position of the larger ion ( $x = d_{lg}/2$ , Figure 10c). Although the electrode potential  $\Psi(0)$  shows a monotonic behavior and negative (because the surface charge is negative), the potentials at contact positions (this is called diffuse layer potential in the case of the restricted primitive model) show a more complex behavior. They remain negative in the small monovalent versus large monovalent case (circles and solid lines). In the *competitive* case (small monovalent vs large divalent), the potential becomes positive only at the contact position of the large divalent cation (squares and dotted lines). When the divalent ion is small, the potential is also positive at the contact of the small ion if the surface charge is large enough.

It is more interesting to plot these potential values as a function of the composition of the electrolyte. Figure 11 shows the values in the *selective* case for  $\sigma = -0.5 \text{ Cm}^{-2}$  and in the *competitive* case for a smaller ( $\sigma = -0.5 \text{ Cm}^{-2}$ ) and a larger ( $\sigma = -1.25 \text{ Cm}^{-2}$ ) surface charge. In the *selective* case (circles with solid lines), even a small amount of small divalent ions is sufficient to change the sign of the potential. The situation in the *competitive* case is much more balanced. At the smaller surface charge (squares and dotted lines), the potential shows a clear sign inversion at the contact of the large ion. At the larger

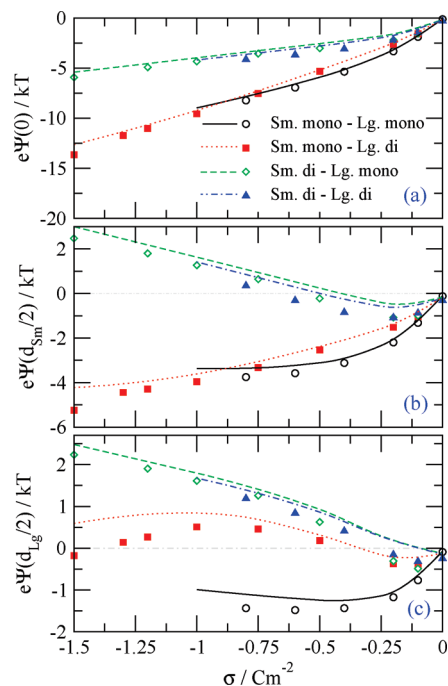


**Figure 10.** Value of mean electrostatic potential (a) at the electrode, (b) at the contact position of the small ion, and (c) at the contact position of the large ion for the four cases listed at Figure 9 as a function of the surface charge. The lines and symbols represent DFT and MC results, respectively.

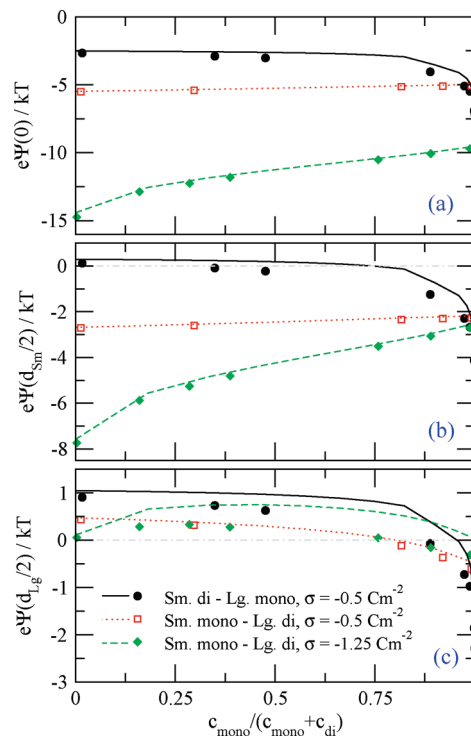


**Figure 11.** Value of mean electrostatic potential (a) at the electrode, (b) at the contact position of the small ion, and (c) at the contact position of the large ion as a function of cation mole fraction. Results are shown for  $\sigma = -0.5 \text{ Cm}^{-2}$  for the small monovalent vs large monovalent (*selective*) and for  $\sigma = -0.5$  and  $\sigma = -1.25 \text{ Cm}^{-2}$  in the small monovalent vs large divalent (*competitive*) cases. The lines and symbols represent DFT and MC results, respectively.

surface charge (diamonds and dashed lines), nevertheless, the  $\Psi(d_{lg}/2)$  potential shows a maximum that is qualitatively reproduced by the DFT.

Kilic et al.<sup>10</sup> report that the differential diffuse layer capacitance as a function of the potential decreases after going through a maximum in some cases as obtained from their modified PB treatment. Capacitances computed on the basis of the potential versus charge data of Figure 10a show some indication of this behavior, but more careful investigation of this phenomenon will be needed.

**3.3. Competition between Volume-Exclusion and Electrostatic Terms of the Chemical Potential.** The above results also show the rich behavior near the interface when both the charge and the size of the counter-ions are varied. Every paper cited in the Introduction points out the competition of repulsive entropic (hard sphere exclusion) and the attractive electrostatic forces as the explanation of the phenomena. The explanation generally does not go beyond stating this, at least, to our best knowledge.

DFT provides a quantitative analysis of this competition because it separates the chemical potential in the following way:

$$\frac{\mu_i(x)}{kT} = \frac{\mu_i^0(x)}{kT} + \log(\rho_i(x)) + \frac{\mu_i^{\text{HS}}(x)}{kT} + \frac{\mu_i^{\text{SC}}(x)}{kT} + \frac{z_i e \Psi(x)}{kT} \quad (14)$$

where the first term on the right-hand side contains the temperature-dependent part of the ideal term (the de Broglie wavelength) plus the effect of the wall. The last terms correspond to the hard sphere exclusion (HS), ionic correlations or screening (SC), and the interaction of the ion with the average electrostatic potential,  $\Psi(x)$ . We call the last term the mean field (MF) term. The sum of the SC and MF terms is called the electrostatic (ES) term. We plot the chemical potential profiles for the various species starting from their contact positions ( $d_i/2$ ).

The specific values of these terms depend on the final result of the DFT calculation; therefore, the values of the various terms will depend on other terms. A total separation of these terms is not possible; they are never independent. Any such analysis is deeply connected to the theory that provides these terms, but this does not decrease the importance of the analysis. Our basic goal is to quantify and illustrate the competition between the entropic and energetic terms. Basically, this competition can be reduced to the competition between the HS and ES terms. Simulations can provide the  $\log(\rho_i)$  term and the MF term straightforwardly. These two terms determine the HS + SC term if the total chemical potential is known (simulated, for example, in the grand-canonical ensemble). The separation of these two terms in simulations is far from trivial. Theories naturally, though not less arbitrarily, do this separation when they express the free energy as a sum of these different terms. The success of the theory justifies this kind of separation. We expect that this separation gives intuitive insight into the mechanism of the competition between the two ionic species.

Because we are interested primarily in the competitive accumulation of the various ionic species at the interface from the bulk, we need to relate our terms of the chemical potential to the bulk values. Because the value of the total chemical potential is independent of  $x$ , we withdraw the bulk values from the  $x$ -dependent parts to obtain

$$\log\left(\frac{\rho_i(x)}{\rho_i^b}\right) = -\frac{\Delta\mu_i^{\text{HS}}(x)}{kT} - \frac{\Delta\mu_i^{\text{SC}}(x)}{kT} - \frac{z_i e \Psi(x)}{kT} \quad (15)$$

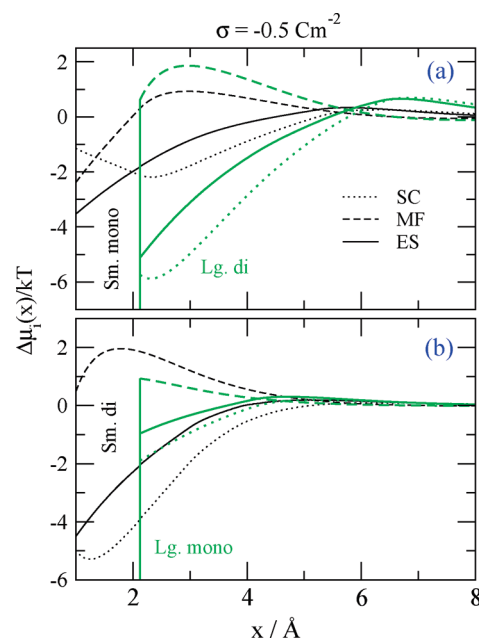


**Figure 12.** SC, MF, and ES terms of the chemical potential referred to bulk for (a) the small monovalent vs large divalent (*competitive*) and (b) the small divalent vs large monovalent (*selective*) cases at  $\sigma = -0.5 \text{ Cm}^{-2}$  surface charge as obtained from DFT. The concentration of the cations is 1 M in every case.

where the quantities denoted by  $\Delta$  mean values compared to the bulk values:  $\Delta\mu_i^{\text{HS}}(x) = \mu_i^{\text{HS}}(x) - \mu_i^{\text{HS,b}}$  and  $\Delta\mu_i^{\text{SC}}(x) = \mu_i^{\text{SC}}(x) - \mu_i^{\text{SC,b}}$ . The last term is the value of the MF term compared also to the bulk because  $\Psi(x) = 0$  in the bulk.

The total electrostatic contribution to the chemical potential can be interpreted as the sum of the SC and the MF contributions (ES). Figure 12 shows these terms for the two limiting cases: the *competitive* (small monovalent vs large divalent, Figure 12a) and the *selective* (large monovalent ions vs small divalent, Figure 12b) cases. This figure gives interesting insight into the electrostatics of the system. In the SC contribution (dotted lines), the electrostatic coupling between ions always tends to be negative; this is an attractive contribution. It generally becomes more negative approaching the interface because the density, and, consequently, the ionic strength increases. In some cases (e.g., small monovalent in the *competitive* case), this term increases in spite of the increasing density approaching the interface (Figure 12a). This is a result of the increasing repulsion of many like-charged ions accumulated at the interface attracted by the large surface charge and favored by entropic advantages. The MF terms show a more complex behavior because this term depends on the mean electrostatic potential  $\Psi(x)$ , which can show a nonmonotonic behavior (due to, for example, *charge inversion* induced by the presence of multivalent ions) as discussed in the preceding subsection. The sum of these two terms (ES) shows a relatively stable behavior (negative and monotonic close to the interface). It intimately depends on the HS term because the sum of these has to give  $\log(\rho_i(x)/\rho_i^b)$ . The relative sizes of the SC, MF, and ES terms do not depend strongly on the surface charge (not shown);  $\sigma$  scales these curves, but their relative sizes are quite unaffected. So the results for  $\sigma = -0.5 \text{ Cm}^{-2}$  shown in Figure 12 are characteristic of other surface charges.

Next we focus on the competition between the HS and the ES terms. We start with those cases where there is no doubt about the winner of the competition. These cases are those when the valence of the larger ion is less than or equal to the valence

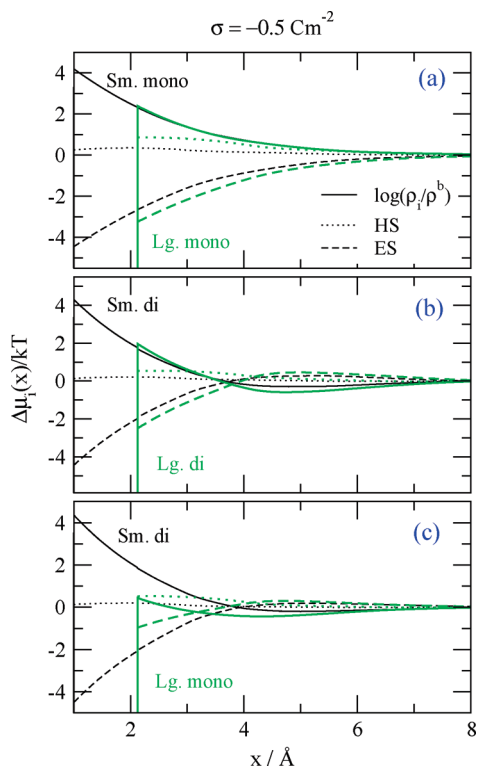


**Figure 13.**  $\log(\rho_i(x)/\rho_i^b)$ , HS, and ES terms of the chemical potential referred to bulk for (a) the small monovalent vs large monovalent, (b) the small divalent vs large divalent, and (c) the small divalent vs large monovalent (*selective*) cases at  $\sigma = -0.5 \text{ Cm}^{-2}$  surface charge as obtained from DFT. The concentration of each of the cations is 1 M in every case.

of the smaller ion (the small monovalent vs large monovalent, small divalent vs large divalent, and small divalent vs large monovalent cases). Figure 13 shows the  $\log(\rho_i(x)/\rho_i^b)$ , the HS, and the ES terms of  $\Delta\mu_i(x)/kT$  for the above three cases at a fixed surface charge  $-0.5 \text{ Cm}^{-2}$ . In this and the next figure, the HS or ES term is more favorable for ionic species  $i$  the more negative it is because then it produces a larger positive  $\log(\rho_i(x)/\rho_i^b)$  term.

In all cases, the small ions are more favorable because they can approach the surface closer as shown by the  $\log(\rho_i(x)/\rho_i^b)$  curves. In spite of the size difference, the HS term seems to play a less-important role. The ES term behaves similarly when the cations have the same valence (Figure 13a and b), whereas it gives additional help to the small divalent cations against the large monovalent ones (Figure 13c).

Figure 14 shows the *competitive* (small monovalent vs large divalent) case that was illustrated in terms of adsorption in Figure 6, in terms of density profiles in Figure 7, and in terms of electrolyte composition in Figure 8. This figure shows the  $\log(\rho_i(x)/\rho_i^b)$ , HS, and ES curves for three characteristic surface charges. For a relatively low surface charge ( $\sigma = -0.5 \text{ Cm}^{-2}$ ), the density at the electrode is not high enough for the HS terms to be important and selectivity is determined mainly by the electrostatic advantage of the divalent ion (Figure 14a). With an increasing surface charge, the density in the DL region and the HS term becomes more positive (Figure 14b and c), whereas the ES terms become more negative. At a large surface charge ( $\sigma = -1.5 \text{ Cm}^{-2}$ , Figure 14c), the HS penalty paid by the large divalent ions (compared to the small monovalent ion) becomes so large that it overcomes the electrostatic advantage (compared to the small monovalent ion). In this case, the small monovalent

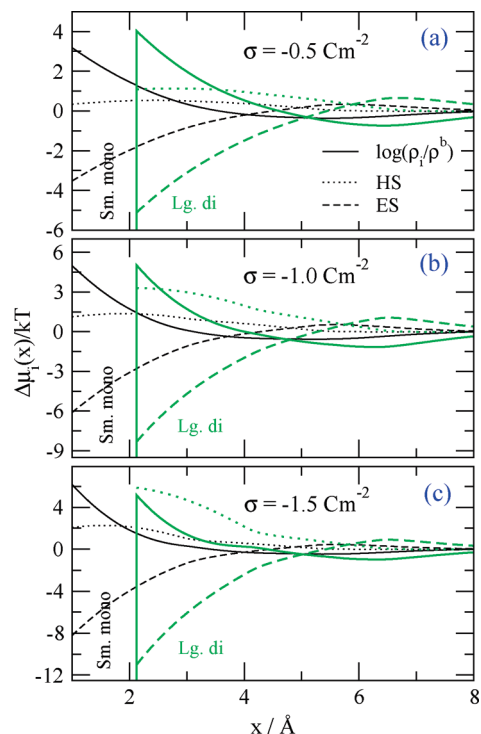


**Figure 14.**  $\log(\rho_i(x)/\rho_i^b)$ , HS, and ES terms of the chemical potential referred to bulk for the small monovalent vs large divalent (*competitive*) case for various surface charges as obtained from DFT. The concentration of each of the cations is 1 M in every case.

cations dominate in the DL region because their small size makes them more able to fit into the densely packed DL region.

Instead of showing many  $\Delta\mu_i(x)$  profiles, it is advantageous to characterize the competition of the various terms by a single number, as we did in the case of the adsorption. Because  $d\mu_i(x)/dx$  can be interpreted as a thermodynamic force, its integral

$$\int_{\infty}^{d_i/2} \frac{d\mu_i(x)}{dx} dx = \int_{\infty}^{d_i/2} d\mu_i = \mu_i(d_i/2) - \mu_i^b = \Delta\mu_i(d_i/2) \quad (16)$$

can be interpreted as the work needed to bring the given ion from bulk into contact position at the interface. This work is a characteristic measure of the free energy that the various ions have to pay (or what they gain) by going from the bulk into contact position. Equation 16 shows that this work is just the contact value of the chemical potential difference introduced in eq 15.

Figure 15a and b shows the contact values of the various terms for both ions in the most interesting *competitive* situation (small monovalent vs large divalent) as a function of the surface charge. A specific  $\Delta\mu_i$  term (HS, ES, SC, or MF) favors the given ionic species if it is negative. The HS term is always positive, so the HS exclusion appears as an obstacle that ions have to surpass to get to the interface. This term is more positive in the case of the large ions (Figure 15b). The SC term, as we noted at Figure 12, is always negative. The MF term, however, shows a more interesting behavior. It is negative for the small cations because the potential is negative at their contact position. In the case of the large divalent cations, nevertheless, this term is positive because the potential is positive at their contact positions because of *charge inversion*. This region is rich in cations: their number is actually larger than would be necessary to neutralize the electrode; that is why a layer of excess anions

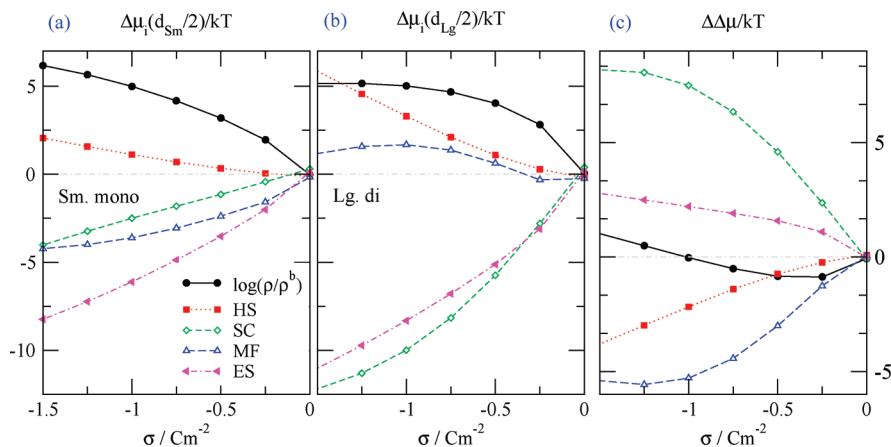


**Figure 15.** Contact values of the relative chemical potentials (the work needed to bring the given ion from bulk into contact position) for the small monovalent vs large divalent (*competitive*) case for (a) the small monovalent cation and (b) the large divalent cation as a function of surface charge. Panel c shows the difference of the values shown in panels a and b. The concentration of each of the cations is 1 M in every case. In this figure, the symbols are used for clarity to distinguish different lines and do not represent MC results.

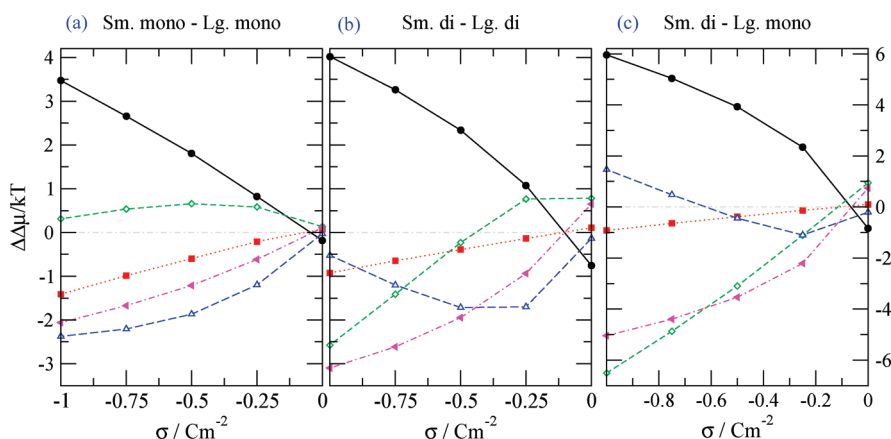


**Figure 16.**  $\Delta\Delta\mu/kT$  results for (a) the small monovalent vs large monovalent, (b) the small divalent vs large divalent, and (c) the small divalent vs large monovalent (*selective*) cases as a function of surface charge. The difference is obtained by subtracting the contact values of the chemical potential terms for the large ion from the corresponding terms for the small ion. The difference (in the cases of the HS, ES, MF, and SC terms) favors the small ion when it is negative, whereas it favors the large ion when it is positive. The concentration of each of the cations is 1 M in every case. In this figure, the symbols are used for clarity to distinguish different lines and do not represent MC results.

appears farther from the electrode. The large cations cannot get close enough to the electrode to enjoy the attractive electrostatic energy of the electrode charge because the small cations screen this attraction. Therefore, the total electrostatic term (ES) is just moderately deeper for the large divalent ion. The HS penalty surpasses this electrostatic advantage at large surface charges and turns the interface *selective* for the small monovalent cations.

The competition of these terms is better seen if we define the difference of the various  $\Delta\mu_i$  terms for the two cations. Specifically, we always define this difference as the term for the small ion minus the term for the large ion:  $\Delta\Delta\mu^{\text{HS}} = \Delta\mu_{\text{Sm.mono}}^{\text{HS}}(d_{\text{Sm}}) - \Delta\mu_{\text{Lg.di}}^{\text{HS}}(d_{\text{Lg}})$  and similarly for the other terms. Therefore, this term favors the small ion if it is negative and favors the large ion if it is positive. In Figure 15c, we plot these curves. The change in the sign of the  $\log(\rho_i(x)/\rho_i^b)$  term shows the change in the selectivity as was shown already in Figure 6. The HS and MF terms favor the small monovalent cations (they are negative). The SC term favors the large divalent cations (it is positive) because the repulsive interaction between the small monovalent ions in their high-density layer near the electrode gives a positive contribution to the integral in eq 16. The balanced competition of all of these terms produces the balanced competition of the two cationic species in this case.

In Figure 16, we characterize the competition in the other three cases (those shown in Figure 13) using the  $\Delta\Delta\mu$  quantities.

In the small monovalent versus large monovalent case (Figure 16a), the SC term favors the large monovalent ion for the same reason described above. The HS term favors the small ion in every case. The MF term favors the small ions because the electrostatic potential is deeper in their contact position (see Figure 9a).

The situation is more complex in the case of two divalent ions (Figure 16b). The SC term also becomes favorable for the small divalent cation because less divalent ions are enough to neutralize the electrode. Thus, the ionic density in the DL region is not very high and the repulsion between cations does not give a large contribution as in the case of small monovalent cations (Figures 15c and 16a). The MF term shows a minimum due to the nonmonotonic behavior of the mean potential that is usual in the presence of divalent ions (Figure 9b–d).

In the *selective* case (small divalent vs large monovalent, Figure 16c), both the HS and ES terms favor the small divalent cation. These two effects strengthen each other and make the interface strongly selective for the small divalent cation.

#### 4. Conclusions

We studied the adsorption of two cationic species at a highly charged planar interface. We concentrated on the selective competition of the two species at the interface inspired by our

similar investigations in an ion channel geometry.<sup>53–55,70–73</sup> The planar geometry made it possible to reduce the problem to one dimension and to quantify the competition between hard sphere exclusion and electrostatic terms by the natural division of the chemical potential in the framework of DFT. The competition of these terms is behind the competition of ions with different size and valence. Our results showed that smaller and divalent ions have an advantage at the interface, whereas in the *competitive* case of small monovalent versus large divalent ions the entropic advantage of the former overcomes the electrostatic advantage of the latter at high enough surface charges.

**Acknowledgment.** It is our pleasure to contribute to the special issue dedicated to the 70th birthday of Professor Keith Gubbins and to tribute his enormous contribution to the field of statistical mechanics of liquids. We are grateful for the support of the Hungarian National Research Fund (OTKA K63322 to DB and MV, OTKA F68641 to MV), NIH grant GM067241 (Bob Eisenberg, PI), and the Rush University Committee on Research (to D.G.). We are grateful for the remarks of Ron Fawcett.

## References and Notes

- (1) Fawcett, W. R. *Liquids, Solutions, and Interfaces*; Oxford University Press: New York 2004.
- (2) Hille, B. *Ionic Channels of Excitable Membranes*; Sinauer Associates: Sunderland, MA 1992.
- (3) Gouy, G. *J. Phys.* **1910**, *9*, 457.
- (4) Chapman, D. L. *Philos. Mag.* **1913**, *25*, 475.
- (5) Stern, O. *Z. Z. Electrochem.* **1924**, *30*, 508.
- (6) Debye, P.; Hückel, E. *Physik* **1923**, *24*, 185.
- (7) Derjaguin, B. V.; Landau, L. *Acta Physicochim. USSR* **1941**, *14*, 633.
- (8) Verwey, E. J. W.; Overbeek, J. Th. G. *Theory of the Stability of Lyophobic Colloids*; Elsevier: Amsterdam, 1948.
- (9) Boda, D.; Fawcett, W. R.; Henderson, D.; Sokolowski, S. *J. Chem. Phys.* **2002**, *116*, 7170.
- (10) Kilic, M. S.; Bazant, M. Z.; Ajdari, A. *Phys. Rev. E* **2007**, *75*, 021502.
- (11) Kilic, M. S.; Bazant, M. Z.; Ajdari, A. *Phys. Rev. E* **2007**, *75*, 021503.
- (12) Bazant, M. Z.; Kilic, M. S.; Storey, B. D.; Ajdari, A. arXiv:cond-mat/0703035
- (13) Bikerman, J. J. *Philos. Mag.* **1942**, *33*, 384.
- (14) Borukhov, I.; Andelman, D.; Orland, H. *Phys. Rev. Lett.* **1997**, *79*, 435.
- (15) Biesheuvel, P. M.; Lyklema, J. *J. Phys.: Condens. Matter* **2005**, *17*, 6337.
- (16) Biesheuvel, P. M.; Leermakers, F. A. M.; Stuart, M. A. C. *Phys. Rev. E* **2006**, *73*, 011802.
- (17) Outhwaite, C. W.; Bhuiyan, L. B. *J. Chem. Soc., Faraday Trans.* **1983**, *79*, 707.
- (18) Woelki, S.; Kohler, H.-H. *Chem. Phys.* **2000**, *261*, 411.
- (19) Woelki, S.; Kohler, H.-H. *Chem. Phys.* **2000**, *261*, 421.
- (20) Di Caprio, D.; Valiskó, M.; Holovko, M.; Boda, D. *Mol. Phys.* **2006**, *104*, 3777.
- (21) Blum, L. *J. Phys. Chem.* **1977**, *81*, 136.
- (22) Henderson, D.; Lebowitz, J. L.; Blum, L.; Waisman, E. *Mol. Phys.* **1980**, *39*, 47.
- (23) Henderson, D.; Blum, L.; Smith, W. R. *Chem. Phys. Lett.* **1979**, *63*, 381.
- (24) Lozada-Cassou, M.; Saavedra-Barrera, R.; Henderson, D. *J. Chem. Phys.* **1982**, *77*, 1472.
- (25) Plischke, M.; Henderson, D. *J. Chem. Phys.* **1988**, *88*, 2712.
- (26) Rosenfeld, Y. *J. Chem. Phys.* **1993**, *109*, 8126.
- (27) Spohr, E. *Electrochim. Acta* **2003**, *49*, 23.
- (28) Deserno, M.; Jiménez-Angeles, F.; Holm, C.; Lozada-Cassou, M. *J. Phys. Chem. B* **2001**, *105*, 10983.
- (29) Mukherjee, A. K.; Schmitz, K. S.; Bhuiyan, L. B. *Langmuir* **2004**, *20*, 11802.
- (30) Lyubartsev, A. P.; Tang, J. X.; Janmey, P. A.; Nordenskiöld, L. *Phys. Rev. Lett.* **1998**, *81*, 5465.
- (31) Allahyarov, E.; Gompper, G.; Löwen, H. *J. Phys.: Condens. Matter* **2005**, *17*, S1827.
- (32) Pelta, J.; Durand, D.; Doucet, J.; Livolant, F. *Biophys. J.* **1996**, *71*, 48.
- (33) Pelta, J.; Livolant, F.; Sikorav, J.-L. *J. Biol. Chem.* **1996**, *271*, 5656.
- (34) Gelbart, W. M.; Bruinsma, R. F.; Pincus, P. A.; Parsegian, V. A. *Phys. Today* **2000**, *53*, 38.
- (35) Burak, Y.; Ariel, G.; Andelman, D. *Biophys. J.* **2003**, *85*, 2100.
- (36) Lobaskin, V.; Qamhieh, K. *J. Phys. Chem. B* **2003**, *107*, 8022.
- (37) Martín-Molina, A.; Quesada-Pérez, M.; Galisteo-González, F.; Hidalgo-Álvarez, R. *J. Phys.: Condens. Matter* **2003**, *15*, S3475.
- (38) Martín-Molina, A.; Maroto-Centeno, J. A.; Hidalgo-Álvarez, R.; Quesada-Pérez, M. *J. Chem. Phys.* **2006**, *125*, 144906.
- (39) Quesada-Pérez, M.; Martín-Molina, A.; Hidalgo-Álvarez, R. *Langmuir* **2005**, *21*, 9231.
- (40) Martín-Molina, A.; Quesada-Pérez, M.; Hidalgo-Álvarez, R. *J. Phys. Chem. B* **2006**, *110*, 1326.
- (41) Delville, A.; Gasmí, N.; Pellenq, R. J. M.; Caillol, J. M.; Van Damme, H. *Langmuir* **1998**, *14*, 5077.
- (42) Jönsson, B.; Wennerström, H.; Nonat, A.; Cabane, B. *Langmuir* **2004**, *20*, 6702.
- (43) Jönsson, B.; Nonat, A.; Labbez, C.; Cabane, B.; Wennerström, H. *Langmuir* **2005**, *21*, 9211.
- (44) Labbez, C.; Jönsson, B.; Pochard, I.; Nonat, A.; Cabane, B. *J. Phys. Chem. B* **2006**, *110*, 9219.
- (45) Wang, K.; Yu, Y.-X.; Gao, G.-H.; Luo, G.-S. *J. Chem. Phys.* **2005**, *123*, 234904.
- (46) Wang, K.; Yu, Y.-X.; Gao, G.-H.; Luo, G.-S. *J. Chem. Phys.* **2007**, *126*, 135102.
- (47) Taboada-Serrano, P.; Yiacoumi, S.; Tsouris, C. *J. Chem. Phys.* **2005**, *123*, 054703.
- (48) Taboada-Serrano, P.; Yiacoumi, S.; Tsouris, C. *J. Chem. Phys.* **2006**, *125*, 054716.
- (49) Valiskó, M.; Henderson, D.; Boda, D. *J. Phys. Chem. B* **2004**, *108*, 16548.
- (50) Gillespie, D.; Valiskó, M.; Boda, D. *J. Phys.: Condens. Matter* **2005**, *17*, 6609.
- (51) Gillespie, D.; Nonner, W.; Eisenberg, R. S. *J. Phys.: Condens. Matter* **2002**, *14*, 12129.
- (52) Gillespie, D.; Nonner, W.; Eisenberg, R. S. *Phys. Rev. E* **2003**, *68*, 031503.
- (53) Nonner, W.; Catacuzzeno, L.; Eisenberg, B. *Biophys. J.* **2000**, *79*, 1976.
- (54) Nonner, W.; Gillespie, D.; Henderson, D.; Eisenberg, B. *J. Phys. Chem. B* **2001**, *105*, 6427.
- (55) Boda, D.; Henderson, D.; Busath, D. D. *J. Phys. Chem. B* **2001**, *105*, 11574.
- (56) Rosenfeld, Y.; Schmidt, M.; Löwen, H.; Tarazona, P. *Phys. Rev. E* **1997**, *55*, 4245.
- (57) Kierlik, E.; Rosinberg, M. L. *Phys. Rev. A* **1991**, *44*, 5025.
- (58) Rosenfeld, Y. *J. Chem. Phys.* **1993**, *98*, 8126.
- (59) Li, Z.; Wu, J. *Phys. Rev. E* **2004**, *70*, 031109.
- (60) Li, Z.; Wu, J. *Phys. Rev. Lett.* **2006**, *96*, 048302.
- (61) (a) Waisman, E.; Lebowitz, J. L. *J. Chem. Phys.* **1970**, *52*, 4307. (b) Waisman, E.; Lebowitz, J. L. *J. Chem. Phys.* **1972**, *56*, 3086. (c) Waisman, E.; Lebowitz, J. L. *J. Chem. Phys.* **1972**, *56*, 3093. (d) Blum, L. *Mol. Phys.* **1975**, *30*, 1529.
- (62) Hiroike, K. *Mol. Phys.* **1977**, *33*, 1195.
- (63) Blum, L.; Rosenfeld, Y. *J. Stat. Phys.* **1991**, *63*, 1177.
- (64) (a) Pizio, O.; Patrykiewicz, A.; Sokolowski, S. *J. Chem. Phys.* **2004**, *121*. (b) Pizio, O.; Patrykiewicz, A.; Sokolowski, S. *Condensed Matter Physics* **2004**, *7*, 779. (c) Pizio, O.; Sokolowski, S. *J. Chem. Phys.* **2005**, *122*, 144707.
- (65) Reszko-Zygmunt, J.; Sokolowski, S.; Henderson, D.; Boda, D. *J. Chem. Phys.* **2005**, *122*, 084504.
- (66) Boda, D.; Chan, K.-Y.; Henderson, D. *J. Chem. Phys.* **1998**, *109*, 1362.
- (67) Henderson, D.; Blum, L.; Lebowitz, J. *J. Electroanal. Chem.* **1979**, *102*, 315.
- (68) Pellenq, R. J.-M.; Caillol, J. M.; Delville, A. *J. Phys. Chem. B* **1997**, *101*, 8584.
- (69) Squires, T. M.; Bazant, M. Z. *J. Fluid. Mech.* **2004**, *509*, 217.
- (70) Boda, D.; Busath, D. D.; Henderson, D.; Sokolowski, S. *J. Phys. Chem. B* **2000**, *104*, 8903.
- (71) Gillespie, D.; Xu, L.; Wang, Y.; Meissner, G. *J. Phys. Chem. B* **2005**, *109*, 15598.
- (72) Boda, D.; Valiskó, M.; Eisenberg, B.; Nonner, W.; Henderson, D.; Gillespie, G. *J. Chem. Phys.* **2006**, *125*, 034901.
- (73) Boda, D.; Valiskó, M.; Eisenberg, B.; Nonner, W.; Henderson, D.; Gillespie, G. *Phys. Rev. Lett.* **2007**, *98*, 168102.